



Cite this: *Energy Environ. Sci.*,
2015, 8, 2371

Received 1st May 2015,
Accepted 26th June 2015

DOI: 10.1039/c5ee01363a

www.rsc.org/ees

A high tap density secondary silicon particle anode fabricated by scalable mechanical pressing for lithium-ion batteries†

Dingchang Lin,^a Zhenda Lu,^a Po-Chun Hsu,^a Hye Ryoung Lee,^b Nian Liu,^a
Jie Zhao,^a Haotian Wang,^c Chong Liu^a and Yi Cui^{*ad}

Much progress has been made in developing high capacity lithium ion battery electrode materials such as silicon anodes. With the powerful nanomaterial design approach, cycle life of silicon anodes has been increased significantly. However, nanomaterials have three major issues to be addressed, including severe side reactions due to a large surface area, low tap density and poor scalability. Nanostructured Si secondary clusters (nano-Si SC) are promising for reducing side reactions and increasing tap density, yet the scalability and tap density could still be further improved. Here, we propose a mechanical approach for SC fabrication to address all the problems. With the mechanical approach, > 20 g of nano-Si SC per batch was produced even at our university lab scale, with > 95% yield. Moreover, much denser packing of nanostructures can be achieved (1.38 g cm⁻³, pellet form), which gives much higher tap density (0.91 g cm⁻³, powder form) and better electrical contact. Accordingly, over 95% of initial capacity is retained after 1400 cycles at 1C, with an average specific capacity of ~1250 mA h g⁻¹. Stable cycling with > 2 mg cm⁻² of areal mass loading (~3.5 mA h cm⁻²) is obtained. After uniformly integrating carbon nanotubes (CNTs) into SCs, intracluster electrical conductivity is further improved. As a result, notably enhanced rate capability is attained, with a high reversible specific capacity of ~1140 mA h g⁻¹ and ~880 mA h g⁻¹ at 2C and 4C, respectively.

Driven by emerging demands for high energy density batteries in consumer electronics and electric vehicles, extensive research has been conducted on high-capacity electrode materials for lithium ion batteries (LIBs).^{1–5} Silicon, with up to 4200 mA h g⁻¹

Broader context

Developing high energy density rechargeable batteries has become a major research topic due to their broad applications in electric vehicles, portable electronics and grid-scale energy storage. The silicon (Si) anode for lithium-ion batteries is attractive because of its ten-time higher theoretical capacity (4200 mA h g⁻¹) compared to its graphite counterpart (370 mA h g⁻¹). In the past, powerful nanotechnology has been developed to solve the critical volume change and pulverization problems, which highly improve its electrochemical performance. However, low tap density, poor scalability and high surface area of nanostructures still severely hinder its application. In this work, a mechanical approach for nanostructured Si fabrication has been developed to solve all the above-mentioned problems. By combining industrially mature mechanical processes, large scale fabrication of a high tap density, low surface area nanostructured Si anode was demonstrated. At the same time, further improved electrochemical performance can be achieved. The developed approach provides a new methodology to commercially produce high tap density, low surface area nanostructured electrode materials with low cost, high yield and high throughput.

theoretical specific capacity as anode material, 10 times higher than its conventional graphite counterpart (370 mA h g⁻¹), has triggered strong scientific and technological interest.^{6–9} However, successful implementation of silicon as anode material has been impeded by the large volume change. Similar to other alloy-type anode materials, a large volume change (~300%) of silicon during (de)alloying limits its cycle life by resulting in pulverization of silicon and continuous formation of a solid–electrolyte interface (SEI).^{10–14} Though pulverization has been successfully resolved by decreasing the size to the nanoscale, a tremendous volume change is unavoidable.^{6,10,15} The repeating volume change not only breaks the interparticle electrical contact, but also destroys the as-formed SEI and exposes the fresh interface, which continuously consumes the electrolyte by side reactions and finally blocks active materials from electron/ion exchange.^{13,14,16} To address these problems, engineered void space and the electrolyte blocking layer were proposed and proven to be very powerful.^{17–26} With built-in void space, silicon nanostructures are allowed to expand and contract without breaking interparticle connection. And the engineered

^a Department of Materials Science and Engineering, Stanford University, Stanford, California 94305, USA. E-mail: yicui@stanford.edu

^b Department of Electrical and Engineering, Stanford University, Stanford, California 94305, USA

^c Department of Applied Physics, Stanford University, Stanford, California 94305, USA

^d Stanford Institute for Materials and Energy Sciences, SLAC National Accelerator Laboratory, 2575 Sand Hill Road, Menlo Park, California 94025, USA

† Electronic supplementary information (ESI) available. See DOI: 10.1039/c5ee01363a

electrolyte blocking layer can maintain a mechanically and chemically stable thin SEI.

Although nanomaterial design has resolved some major problems and immensely extended cycle life, other challenges still exist regarding the nanostructured electrodes. In the nanostructured silicon anode, the largely exposed surface results in severe side reactions which lowers Coulombic efficiency. The reduced size scale also creates more interparticle space and surface, giving rise to low tap density and high interparticle resistance, respectively. The low tap density causes low volumetric capacity, thicker electrodes and longer electron pathway for the same mass loading. The large interparticle resistance creates barrier for the electron transport between current collector and active materials. These factors altogether hinder the achievement of high areal mass loading with nanoparticles.

Recently, we present a solution by forming pomegranate-like micrometer-sized secondary clusters (SC) with a nanostructured building block.²⁷ It not only reduces the surface area without sacrificing the superiority of nanostructure, but builds up the conducting framework among nanoparticles for improving electrical conductivity. As a great demonstration, pomegranate-like structure produced by micro-emulsion has proved high Coulombic efficiency as well as impressive areal mass loading with CNT network.²⁷ However, there are still several critical issues remain to be solved. Firstly, the density of SC is still not high enough due to the weak packing force created by solvent evaporation, with resulting tap density of 0.53 g cm^{-3} . Much higher packing density is strongly desired. Secondly, scalability, yield and manufacturing efficiency are still far from practical requirement. To the best of our knowledge, few works, if any, have reported either the fabrication of nanostructured silicon anode with extremely high packing density or economical synthesis processes with excellent industrial compatibility. Here, we demonstrate a general strategy for the nanostructured SC synthesis to address the multifaceted problems. In contrast to conventional strategy which assembles nanostructures directly

to micrometer-sized SC, bulks are firstly made based on nanostructures with high pressure dry press (HPDP). Afterwards, bulks are further broken into micrometer-sized powder with high energy mechanical milling (HEMM). This approach has several distinguished advantages. First of all, both of the techniques are industrially mature. Neither of them calls for elaborate nanostructured assembly. As a consequence, high yield, mass production and efficient manufacture can be expected. Even at our university lab scale, we achieved $>20 \text{ g}$ of final product per batch fabrication, with yield higher than 95%. Secondly, the techniques exhibit high flexibility for SC synthesis. In dry press, density of bulk is tunable by simply varying the applied pressure, while the average size of SC can be easily controlled by HEMM power and time. Moreover, since the approach is based on mechanical processes, it can be applied to a broad range of materials, regardless their surface properties which are sensitive in solvent-based assembly.^{27–30} Above all, mechanical pressure offers an opportunity to produce high packing density of nanostructures. It has been reported that mechanical pressure can give up to 60–70% of fractional volume compaction in as-obtained pellets,³¹ which is the most efficient approach to produce ultrahigh-density packing of solids. In this work, high density (up to 1.38 g cm^{-3}) is produced under $\sim 100 \text{ MPa}$. This is critical for building up closely-packed carbon frameworks and their tight connection with silicon. As a consequence, more than 95% of initial capacity is retained after 1400 cycles at 1C, with average specific capacity $\sim 1250 \text{ mA h g}^{-1}$. Stable cycling of electrode with $>2 \text{ mg cm}^{-2}$ is obtained without CNT additive. In contrast to other solvent-based SC assembly, the mechanical-based techniques provide more opportunities for modifying SC structures. Here, by uniformly integrating CNTs into SC, further improved intracluster electrical conductivity and consequently notable enhanced rate capability can be attained, with specific capacity $\sim 1140 \text{ mA h g}^{-1}$ and $\sim 880 \text{ mA h g}^{-1}$ at 2C and 4C, respectively.

Fig. 1a schematically illustrates the major procedures we performed for micrometer-sized SC synthesis through the

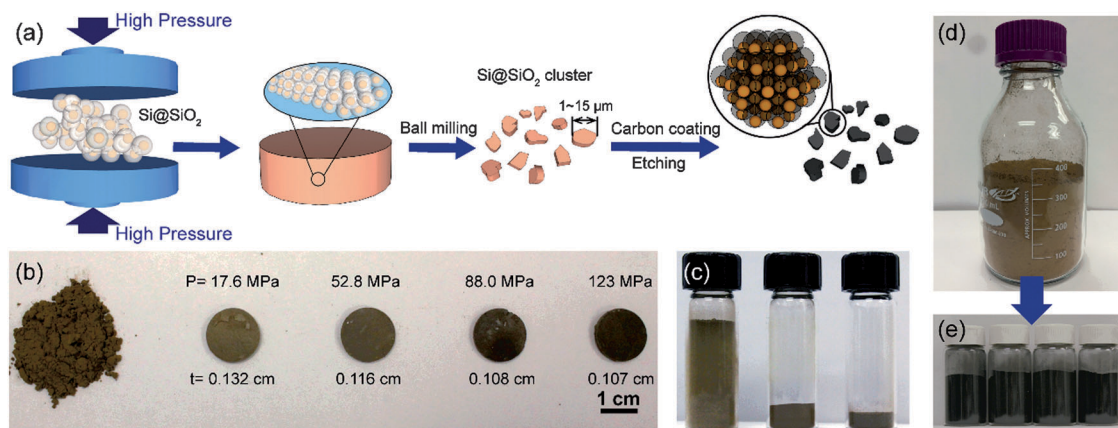


Fig. 1 Mechanical fabrication of the nanostructured silicon (nano-Si) secondary cluster. (a) Schematic illustration of the mechanical-based nano-Si SC fabrication process. (b) Produced pellets under various pressures and their evolution of thickness under increasing applied pressure. Left shows the pristine powder before pressing. Each contains 0.25 g of Si@SiO_2 . (c) Volume comparison on 0.4 g samples in 4 mL vials. From left to right, Si nanoparticle, micro-emulsion produced cluster, and mechanically produced cluster, respectively. (d) Starting materials of Si@SiO_2 powders. (e) 20.12 g of final product (bottom) produced at lab scale from starting powders shown in (d).

mechanical approach. With silica-coated silicon nanoparticles ($\text{Si}@\text{SiO}_2$, overall ~ 150 nm diameter in average) as starting materials synthesized as in our previous study,^{20,27} we firstly exerted mechanical pressure to produce bulk pellets (2nd state in Fig. 1a) which consists of densely packed $\text{Si}@\text{SiO}_2$ nanostructures. Afterwards, bulk pellets are broken into micrometer-sized SC's with HEMM. By controlling the milling time (5 to 40 minutes), we are able to produce the SCs with desired size in the range of 1–15 μm , which is suitable for later cell manufacturing processes with small enough surface exposure. It is noted that before HEMM process, calcining the pellets at 600 $^\circ\text{C}$ for 2 hours is crucial for mechanical stability of the clusters by bridging neighboring nanoparticles together through thermal sintering, which prevents the clusters from breaking into free nanoparticles in the later processes. After powder of SC's was obtained, carbon coating³² was exerted to build up conducting framework, and hydrofluoric acid etching was performed to remove SiO_2 sacrificing layer for engineered void space.

To gain pellets with high packing density, different pressures were tested to study the density evolution with increased pressure. As shown in Fig. 1b, with various pressures from 17.6 MPa to 123 MPa applied on $\text{Si}@\text{SiO}_2$ (0.25 g each), the volume of the particles tremendously shrunk compared to their powder counterpart shown on the very left. It is noted that, with higher pressure, the color of pellet gets darker, indicating denser packing of nanostructures. For the pellets obtained under different pressures, their thicknesses were measured with micrometer screw gauge. It shows that at low pressure region, from 17.6 MPa to 88 MPa, the thickness drops from 0.132 cm to 0.108 cm as pressure increases, which indicates remarkable density augmentation from 1.11 g cm^{-3} to 1.36 g cm^{-3} . However, further increase of applied pressure from 88 MPa to 123 MPa does not increase the density significantly (1.38 g cm^{-3} at 123 MPa). The evolution trend of density *versus* applied pressure is summarized in Fig. S1 (ESI[†]). This indicates that >88 MPa is large enough to achieve densely-packed nanostructures. After HEMM, the as-obtained powders still maintain high tap density. In Fig. 1c, tightly packed pristine Si nanoparticle, SC of Si produced by micro-emulsion as in our previous study,²⁷ and that produced by mechanical process, are shown from left to right, respectively, in 4 mL glass vials. Each vial contains 0.4 g of powders. As is shown, shrunk volume can be observed with micro-emulsion approach, resulting in tap density augmentation from 0.15 g cm^{-3} to 0.53 g cm^{-3} . By the mechanical approach, even higher tap density, up to 0.91 g cm^{-3} can be produced, which almost doubles the value of that produced by its micro-emulsion counterpart.

In the past, few works, if any, have proven the potential mass production of nanostructured silicon anodes with high yield, mass production and superior manufacturing efficiency. At lab scale, hundreds of milligrams of sample were typically made for research purpose. Even though high performance has been achieved, few techniques can be employed to scale up economically. Since mechanical-based HPDP and HEMM are known to be scalable, the process provides opportunities for synthesis far beyond what lab scale achieved before. Here, we show that even at lab scale, over 20 g per batch of final product (Fig. 1e) can be

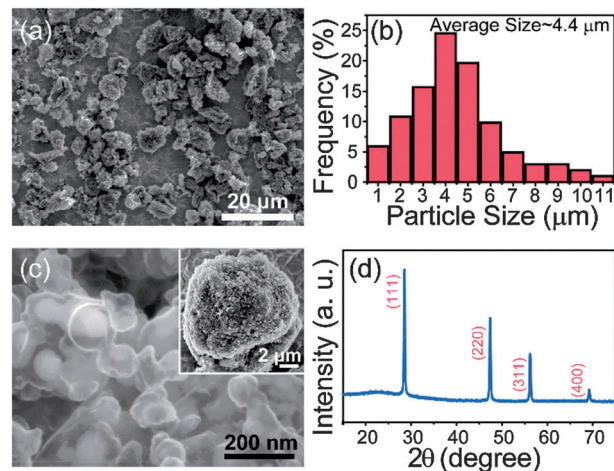


Fig. 2 Characterization of nano-Si SC. (a) Low-magnification SEM image showing the size distribution of SC. (b) Statistical analysis of the distribution of SCs' size based on (a). (c) Magnified SEM image of the surface of SC showing the well-defined void space as well as intact carbon framework. Inset image shows one typical cluster. (d) X-ray diffraction pattern of as-obtained nano-Si SC powders.

produced from $\text{Si}@\text{SiO}_2$ starting powder (Fig. 1d). Moreover, the HPDP and HEMM are so efficient that both can finish processing a large amount of materials in minutes. This is hard to be achieved by solvent-based methods.

To evaluate the size and structure, scanning electron microscopy (SEM) and X-ray diffraction (XRD) of as-obtained SC were performed (Fig. 2). According to the low magnification SEM image (Fig. 2a) and the corresponding statistical analysis (Fig. 2b), the size of SCs shown here varies from 1 μm to 11 μm , with average diameter of $\sim 4.4\text{ }\mu\text{m}$, which is among the preferred range for electrode fabrication. Diverse size here exhibits good capability for dense electrode preparation. Rather than packing uniform SCs which will leave large interstitial volume, diverse size helps efficient occupation by filling interstitial space with smaller SCs. In addition, the survival of nanostructure in mechanical processes is of great importance. Fig. 2c shows the magnified image of a typical SC's (inset of Fig. 2c) surface. As it illustrates, silicon nanoparticles are well coated by carbon shells, with rare free silicon exposed. Inside the carbon shells, void space was left off to adapt volume expansion. This guarantees stable electrode structure and thin SEI layer on SC's outer surface. Typical XRD pattern is also shown in Fig. 2d. The characteristic peaks indicate the crystalline phase of Si nanoparticles as active materials.

With well-established SCs built from optimized nanostructures, superior electrochemical performance can be attained. Here, electrochemical properties were evaluated with galvanostatic cycling between 1 V and 0.01 V. Specific capacity was calculated based on the total weight of silicon nanoparticles and carbon framework. As shown in Fig. 3a, stable cycling of battery for 1400 cycles with $\sim 95\%$ of capacity retention is obtained at 1C (4.2 A g^{-1}) for the capacity loading of $\sim 0.25\text{ mA h cm}^{-2}$ ($\sim 0.2\text{ mg Si per cm}^2$). This indicates that enough void space ($\sim 350\%$) allowing for large volume expansion is of great importance for stable cycle life. In contrast, when not enough

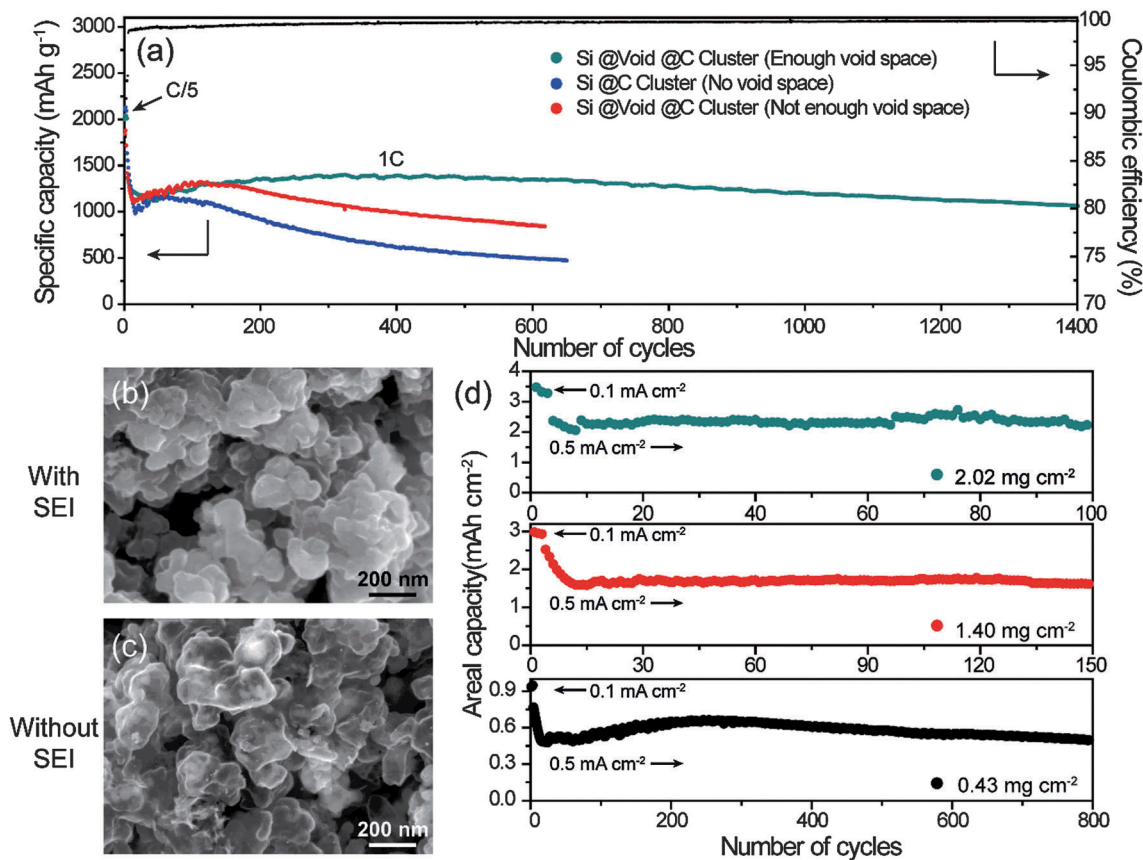


Fig. 3 Electrochemical characterization of nano-Si SC. (a) Delithiation cycling performance and Coulombic efficiency of nano-Si SC at the first 1400 galvanostatic cycles and other structures tested under the same conditions. Rate was set at C/5 for the first 3 cycles and 1C for later cycles. (1C = 4.2 A g⁻¹ of SC). (b) Typical SEM image of nano-Si SC surface after 200 deep cycles with SEI. (c) Corresponding SEM image with SEI removed. (d) Cycling performance of different areal mass loading cell. All electrodes were run at 0.1 mA cm⁻² for the first 3 cycles and 0.5 mA cm⁻² for later cycles.

void space (Si volume to void space = 1:1) is established (Fig. 3a), capacity faded much faster. Samples without any void space were even worse, with only ~50% of initial capacity after 600 cycles. It is noted that the first Coulombic efficiency has also been highly improved here when compared to a previously reported nanosized Si anode.^{20–23} In Fig. S4 (ESI[†]), normalized first cycle voltage profiles of Si SC with different carbon ratios are shown to indicate the first Coulombic efficiency. As is shown, with ~6 wt% of carbon in the structure, close to 80% of first Coulombic efficiency can be obtained.

The strong interparticle connection as well as stable SEI contributes to the superior cycle life. To study the SEI formation, surfaces of SC before and after the removal of SEI are compared here. Hydrochloric acid can be used to etch most of the inorganic components in SEI such as Li₂O, LiF and Li₂CO₃ while it can simultaneously break the stable SEI layer and facilitate the removal of the other insoluble components. As shown in Fig. 3b and c, which refer to the as-obtained surface of SC after 200 deep cycles and its counterpart with SEI removed by diluted hydrochloric acid solution, respectively, there is no significant change on the particle size before and after removal of SEI layer, indicating that thin and stable layers of SEI are formed on the outer carbon shell. Besides, no morphological

change on carbon shell can be observed, which implies the notable impact of engineered void space on preventing structural collapse during cycles.

The capability for high areal mass loading is another advantage of the structure. With mechanical-based techniques, denser packing in SC and further improved electrical conductivity can be expected. These are known to be critical features for high areal mass loading. In the past, though high areal mass loading has been achieved for SC electrodes, CNT network is still needed to build up efficient electron transfer among SCs.²⁷ Here, with improved packing density and electrical conductivity, areal mass loading as high as 2.02 mg cm⁻³ without addition of CNT can be achieved with high areal capacity of ~3.5 mA h cm⁻² at current density of 0.1 mA cm⁻² (Fig. 3d). At increased current density of 0.5 mA cm⁻², we can still retain ~2.3 mA h cm⁻² with stable cycle for > 100 cycles without capacity decay.

When the size increased to the micrometer-scale, conductivity inside the SC unavoidably becomes an issue. The conducting carbon frameworks, which mostly consist of amorphous carbon, generally have poor electrical conductivity.³³ The nanoparticles deep inside the SC may not be fully activated especially under high rate, which partially contributes to the significant specific capacity drop with increased rate. As such, introducing one dimensional

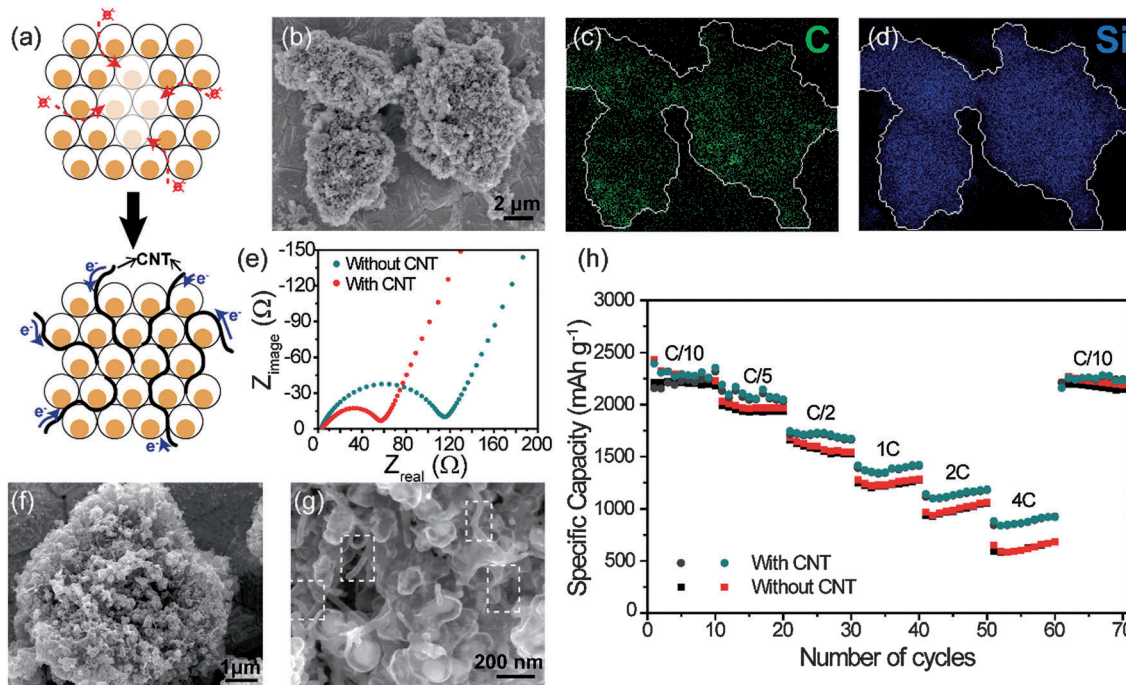


Fig. 4 CNT-embedded nano-Si SC for improved intracluster conductivity. (a) Schematically shows electron transport in SC with and without CNTs. CNTs assist radial electron transport and activate more active materials. (b) SEM image of SC before carbon coating. Corresponding energy-dispersive X-ray spectroscopy maps of (c) carbon distribution and (d) silicon distribution. (e) Nyquist plots of nano-Si SC with/without embedded CNTs after the completion of first delithiation. (f) Typical SEM image of CNT-embedded nano-Si SC. (g) Magnified SEM image showing surface distribution of CNTs and Si nanostructures. (h) Rate capability of SC with/without embedded CNTs with various rates from C/10 to 4C.

conducting pathway into SC's will be helpful for improving intracluster electrical conductivity. As shown schematically in Fig. 4a, with the sole carbon framework, electrons may not be able to efficiently transport into the center of SC, especially at a high rate. With embedded multi-wall CNT, which is known to be good one dimensional electron conductor, efficient electron transport pathways can be built up inside the clusters. Together with local electron transport through carbon framework, more silicon nanoparticles in a SC can be activated. Here, mechanical-based processes are proven to be efficient for uniform addition of CNT into SC's by mixing CNT with Si nanoparticles before mechanical pressing (see Methods in ESI† for details). SEM image and corresponding energy-dispersive X-ray spectroscopy (EDX) mappings of CNT-embedded SC without carbon coating are shown in Fig. 4b. The carbon and silicon mapping all show that CNTs and silicon nanostructures are uniformly spread in the SC. Fig. 4f shows the final SC with CNTs and carbon framework. The magnified image of its surface (Fig. 4g) indicates that CNTs, labeled with dash rectangles in the image, are uniformly dispersed in SCs, providing extra links among Si nanostructures.

The embedded CNTs in SC further improve the electrical conductivity of the electrode. This is supported by electrochemical impedance spectroscopy (EIS) carried out after the completion of the first cycle at the fully delithiated state (held at 1 V vs. Li⁺/Li). According to previous studies, a semicircle of Nyquist plots at the high-frequency region is a good indication of the resistance at the Ohmic surface layer.³⁴ As shown in Fig. 4e,

with the integration of CNTs in SC, the interparticle contact resistance drops significantly, almost half the value of unmodified SC. This result is in good agreement with the rate capability of these cells. Fig. 4h shows the rate capability of cells with and without embedded CNTs in SC. The rate capability is measured with same discharge/charge rate in each cycle and rate is calculated based on theoretical capacity of Si (1C = 4.2 A g⁻¹). It is noted that even without embedded CNTs, good rate capability has been obtained, with ~950 mA h g⁻¹ of specific capacity at 2C and ~500 mA h g⁻¹ at 4C. This suggests that with dense packing and good interparticle connection induced by HPDP, the interparticle resistance has been highly reduced in the whole structure. With embedded CNTs in SC, rate capability is further improved. Specific capacity as high as 1140 mA h g⁻¹ and 880 mA h g⁻¹ can be obtained at 2C and 4C, respectively. This noticeable improvement further supports that embedded CNTs indeed enhance electrical conductivity in SCs and activate more silicon at the center.

From the electrochemical performance point of view, significant improvements in areal mass loading and rate capability have been demonstrated. High areal mass loading > 2 mg cm⁻² is achieved without the addition of any CNTs as conductive additive, which doubles the value that can be obtained before.²⁷ This improvement can be attributed to the increased packing density by mechanically pressing and thus the improved interparticle electrical conductivity inside clusters. The improvement in interparticle electrical conductivity also contributes to the enhanced rate capability. It is noted that, without embedded

CNTs, the rate capability is already better than similar structure fabricated by solution process.²⁷ By pressing CNTs networks into clusters, even better interparticle electrical conductivity is attained and further improvement in rate capability is achieved (from ~ 500 mA h g^{-1} to ~ 880 mA h g^{-1} at 4C).

In summary, a general approach is developed to fabricate densely packed SC using a scalable, industrially compatible, and efficient approach. Rather than using elaborate solvent-based assembly reported before, an industrially-mature mechanical-based approach is introduced here. This can not only be broadly used for solid materials regardless of the surface properties, but also provides more opportunities for tuning the packing density and SC's size. With this approach, even better battery performance is achieved. At the rate of 1C, 1400 stable cycles with an average specific capacity of ~ 1250 mA h g^{-1} is attained, with $>95\%$ initial capacity retained. Moreover, mass loading >2 mg cm^{-2} and capacity loading ~ 3.5 mA h cm^{-2} are achieved without CNTs. With the solvent-free process, introducing a broad range of additives for SC modification becomes efficient. As a demonstration, CNTs were uniformly integrated into the SC to improve the intracluster electrical conductivity. With CNTs embedded, SC shows highly improved rate capability, with ~ 1140 mA h g^{-1} and ~ 880 mA h g^{-1} at 2C and 4C, respectively. We believe that, by combining with economic nanoparticle synthesis³⁵ and pre-lithiation techniques,^{36,37} the scalable, industrially compatible and generally applicable approach we developed for densely-packed nanostructured anode materials will open up a promising opportunity for the forthcoming low-cost and high energy density batteries.

Acknowledgements

Y.C. acknowledges the support from the Assistant Secretary for Energy Efficiency and Renewable Energy, Office of Vehicle Technologies of the U.S. Department of Energy under the Battery Materials Research (BMR) Program.

References

- 1 J. M. Tarascon and M. Armand, *Nature*, 2001, **414**, 359–367.
- 2 M. Armand and J. M. Tarascon, *Nature*, 2008, **451**, 652–657.
- 3 J. B. Goodenough and Y. Kim, *Chem. Mater.*, 2009, **22**, 587–603.
- 4 J. R. Szczech and S. Jin, *Energy Environ. Sci.*, 2011, **4**, 56–72.
- 5 Y. K. Jeong, T.-W. Kwon, I. Lee, T.-S. Kim, A. Coskun and J. W. Choi, *Energy Environ. Sci.*, 2015, **8**, 1224–1230.
- 6 C. K. Chan, H. Peng, G. Liu, K. McIlwrath, X. F. Zhang, R. A. Huggins and Y. Cui, *Nat. Nanotechnol.*, 2008, **3**, 31–35.
- 7 A. Magasinski, P. Dixon, B. Hertzberg, A. Kvit, J. Ayala and G. Yushin, *Nat. Mater.*, 2010, **9**, 353–358.
- 8 H. Kim, B. Han, J. Choo and J. Cho, *Angew. Chem.*, 2008, **120**, 10305–10308.
- 9 W.-J. Zhang, *J. Power Sources*, 2011, **196**, 13–24.
- 10 J. O. Besenhard, J. Yang and M. Winter, *J. Power Sources*, 1997, **68**, 87–90.
- 11 L. Y. Beaulieu, K. W. Eberman, R. L. Turner, L. J. Krause and J. R. Dahn, *Electrochem. Solid-State Lett.*, 2001, **4**, A137.
- 12 M. N. Obrovac and L. Christensen, *Electrochem. Solid-State Lett.*, 2004, **7**, A93.
- 13 D. Aurbach, *J. Power Sources*, 2000, **89**, 206–218.
- 14 C. K. Chan, R. Ruffo, S. S. Hong and Y. Cui, *J. Power Sources*, 2009, **189**, 1132–1140.
- 15 M. T. McDowell, I. Ryu, S. W. Lee, C. Wang, W. D. Nix and Y. Cui, *Adv. Mater.*, 2012, **24**, 6034–6041.
- 16 P. Verma, P. Maire and P. Novák, *Electrochim. Acta*, 2010, **55**, 6332–6341.
- 17 Y. Yao, M. T. McDowell, I. Ryu, H. Wu, N. Liu, L. Hu, W. D. Nix and Y. Cui, *Nano Lett.*, 2011, **11**, 2949–2954.
- 18 H. Wu, G. Chan, J. W. Choi, I. Ryu, Y. Yao, M. T. McDowell, S. W. Lee, A. Jackson, Y. Yang, L. Hu and Y. Cui, *Nat. Nanotechnol.*, 2012, **7**, 310–315.
- 19 H. Wu, G. Zheng, N. Liu, T. J. Carney, Y. Yang and Y. Cui, *Nano Lett.*, 2012, **12**, 904–909.
- 20 N. Liu, H. Wu, M. T. McDowell, Y. Yao, C. Wang and Y. Cui, *Nano Lett.*, 2012, **12**, 3315–3321.
- 21 X. Li, P. Meduri, X. Chen, W. Qi, M. H. Engelhard, W. Xu, F. Ding, J. Xiao, W. Wang, C. Wang, J.-G. Zhang and J. Liu, *J. Mater. Chem.*, 2012, **22**, 11014–11017.
- 22 S. Chen, M. L. Gordin, R. Yi, G. Howlett, H. Sohn and D. Wang, *Phys. Chem. Chem. Phys.*, 2012, **14**, 12741–12745.
- 23 Y. Park, N.-S. Choi, S. Park, S. H. Woo, S. Sim, B. Y. Jang, S. M. Oh, S. Park, J. Cho and K. T. Lee, *Adv. Energy Mater.*, 2013, **3**, 206–212.
- 24 H. Wu and Y. Cui, *Nano Today*, 2012, **7**, 414–429.
- 25 Y. Yao, K. Huo, L. Hu, N. Liu, J. J. Cha, M. T. McDowell, P. K. Chu and Y. Cui, *ACS Nano*, 2011, **5**, 8346–8351.
- 26 W. J. Lee, T. H. Hwang, J. O. Hwang, H. W. Kim, J. Lim, H. Y. Jeong, J. Shim, T. H. Han, J. Y. Kim, J. W. Choi and S. O. Kim, *Energy Environ. Sci.*, 2014, **7**, 621–626.
- 27 N. Liu, Z. Lu, J. Zhao, M. T. McDowell, H.-W. Lee, W. Zhao and Y. Cui, *Nat. Nanotechnol.*, 2014, **9**, 187–192.
- 28 D. S. Jung, T. H. Hwang, S. B. Park and J. W. Choi, *Nano Lett.*, 2013, **13**, 2092–2097.
- 29 Z. Lu and Y. Yin, *Chem. Soc. Rev.*, 2012, **41**, 6874–6887.
- 30 P. J. Bruinsma, A. Y. Kim, J. Liu and S. Baskaran, *Chem. Mater.*, 1997, **9**, 2507–2512.
- 31 A. R. Cooper and L. E. Eaton, *J. Am. Ceram. Soc.*, 1962, **45**, 97–101.
- 32 N. Li, Q. Zhang, J. Liu, J. Joo, A. Lee, Y. Gan and Y. Yin, *Chem. Commun.*, 2013, **49**, 5135–5137.
- 33 D. Dasgupta, F. Demichelis and A. Tagliaferro, *Philos. Mag. B*, 1991, **63**, 1255–1266.
- 34 R. Ruffo, S. S. Hong, C. K. Chan, R. A. Huggins and Y. Cui, *J. Phys. Chem. C*, 2009, **113**, 11390–11398.
- 35 N. Liu, K. Huo, M. T. McDowell, J. Zhao and Y. Cui, *Sci. Rep.*, 2013, **3**, 1919.
- 36 N. Liu, L. Hu, M. T. McDowell, A. Jackson and Y. Cui, *ACS Nano*, 2011, **5**, 6487–6493.
- 37 J. Zhao, Z. Lu, N. Liu, H.-W. Lee, M. T. McDowell and Y. Cui, *Nat. Commun.*, 2014, **5**, 5088.